ARTICLE

Optical and Electrochemical Properties of Spirobifluorene Iridanaphthalene Complexes

Received 00th January 20xx,
Accepted 00th January 20xx

DOI: 10.1039/x0xx00000x

Maria Talavera,[a,*] Raquel Pereira-Cameselle,[b] Ángeles Peña-Gallego,[c] Irene Vázquez-Carballo,[a] Inmaculada Prieto,[c,d] J. Lorenzo Alonso-Gómez[b] and Sandra Bolaño[a,*]

Three new spirobifluorene iridaaromatic compounds bearing electron-withdrawing or electron-donor substituents or another iridanaphthalene moiety have been synthesized and structurally characterized. Thorough experimental and theoretical evaluation revealed that these novel systems present a high thermal, air and electrochemical stability as well as low optical and electronic energy gap values with a significant redshift of the absorption maximum in the UV-Vis spectra and predicted remarkably higher first hyperpolarizabilities compared to their organic counterparts. Therefore, the combination of a metallaaromatic system with a spirobifluorene moiety leads to the design and development of new spirobifluorene derivatives. These new systems have shown interesting optical and electronic properties making them of interest for future applications in optoelectronics.

Introduction

In the last decade, the chemistry of metallaaromatic compounds has grown extensively, and new structures are known, including those in which the substitution of a carbon atom by a transition metal transforms a non-aromatic organic compound into an aromatic one.[1-6] The interest in the metallaaromatic compounds is not only focused on their aromatic and organometallic reactivity but also on the study of their optical, electronic and thermal properties with a view to their application in molecular materials and devices.[7-13]

Besides, organic molecules with a non-centrosymmetric electronic structure, high thermal and morphological stability and charge transfer capacity, such as allenes or spirobifluorene derivatives have taken attention in recent years.[14, 15] These characteristics together with their high polarizability grant them second-order NLO properties which are of great interest for applications in optical and electro-optical devices, photodynamic therapy or biological imaging.[16-21]

In this regards, our group developed the synthesis of the first spirobifluorene metallaaromatic complex which showed aromaticity, high thermal stability and UV-Vis absorptivity.[22] However, studies on NLO and electrochemical properties were not performed. Despite of the potential of organometallic complexes in this area,[23-28] the optical and electrochemical properties of transition metal metallaaromatic complexes forming part of the π-skeleton of an organic molecule with a non-centrosymmetric electronic structure have been barely studied.

For these reasons, this work focuses on the effect on the properties of the systems due to the introduction of another iridaaromatic system or electron donor/acceptor substituents at spirobifluorene iridaaromatic structures. Consequently, new spirobifluorene complexes, including the first spirobifluorene structure containing two iridaaromatic systems, have been synthesized. Additionally, experimental evaluation of their thermal stability, optical and electrochemical properties as well as a theoretical analysis of their aromaticity and hyperpolarizability has been performed.

Results and discussion

The synthetic procedure used for the synthesis of the spirobifluorene iridanaphthalene complex **1** reported in the literature[22] was also used for the compounds under study (Chart 1). Thus, for complex **2** the dipropargylic alcohol **III**, substituted at two different branches of the spirobifluorene moiety, was synthesized while for complexes **3** and **4** propargylic alcohols with a ketone (**II**) or a methoxyphenyl group (**VI**), respectively, were obtained from their respective ketones (see SI for further details). The reactivity of these compounds with one or two equivalents of [IrCp*Cl(NCMe)(PMe_3)]PF_6 in methanol led to the corresponding methoxyalkenylcarbene iridium complex which followed an intramolecular C–H bond activation at the spirobifluorene moiety to give the iridaaromatic compounds (Scheme 1 and SI). The complexes under study are based on a 2,2'-substituted spirobifluorene. Thus, two iridanaphthalene

[a] *Universidade de Vigo, Departamento de Química Inorgánica, Campus Universitario, 36310, Vigo, Spain*
[b] *Universidade de Vigo, Departamento de Química Orgánica, Campus Universitario, 36310, Vigo, Spain*
[c] *Universidade de Vigo, Departamento de Química Física, Campus Universitario, 36310, Vigo, Spain*
[d] *Metallosupramolecular Chemistry Group Galicia South Health Research Institute (IIS Galicia Sur) SERGAS-UVIGO. Galicia – Spain*
E-mails: bgs@uvigo.es, matalaveran@uvigo.es

† Electronic Supplementary Information (ESI) available: Full characterization, NMR spectra, UV-Vis, CV and DFT details and XYZ coordinates. See DOI: 10.1039/x0xx00000x

moieties can be part of the π-skeleton of the two orthogonal fluorene branches (**2**), or an iridanaphthalene moiety in one of the branches and a ketone as an acceptor group (**3**) or methoxyphenyl as a donor substituent (**4**) in the other branch (Chart 1).

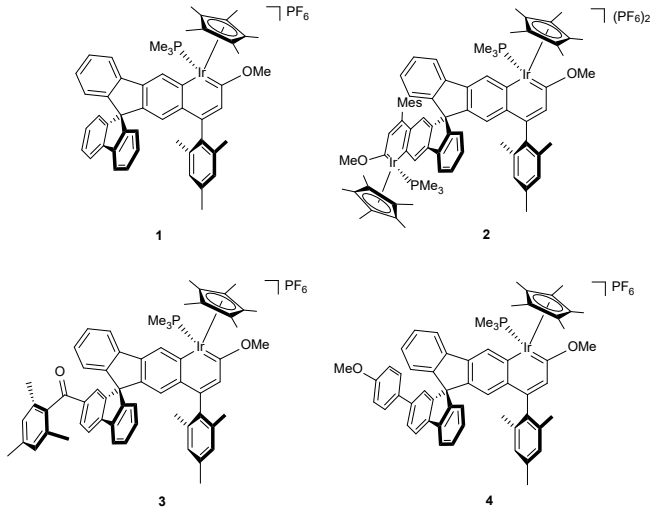

Chart 1. Molecular structure of one of the possible stereoisomers of each complex under study.All the complexes are soluble in organic solvents such as CH_2Cl_2, THF, MeOH or CH_3CN and stable under air in both solution and solid state for months.

The complexes under study were characterised by NMR spectroscopy and high-resolution mass spectrometry and X-ray diffraction analysis for **2** and **3** where adequate monocrystals were obtained (see supporting information). The aromaticity of the complexes **2**-**4** is supported by the downfield shift of the H_β between 6.50-6.70 ppm, in the range of the aromatic protons of the mesityl groups of all the complexes (6.60-6.80 ppm) and the protons in *ortho* to the methoxy substituent in the methoxyphenyl ring of complex **3** (6.61-6.67 ppm) In addition, all the NMR data is in accordance to previously studied metallaaromatic complexes.[22, 29-32] The chiral nature of the iridium centre and the 2,2'-disubstituted SBF moiety, provides different diastereoisomers for complexes **2**-**4**. On the one hand, compound **2** can present three pairs of enantiomers (*R,P,R*)/(*S,M,S*)-**2**, (*S,P,S*)/(*R,M,R*)-**2** and (*R,P,S*)/(*S,M,R*)-**2**, due to the presence of two chiral iridium atoms (*R,S* centres) and the chiral axis of the spirobifluorene ligand (*M,P* isomers). The ^1H and $^{13}C\{^1H\}$ NMR spectra confirm the mixture of diastereoisomers in a 2:1:1 ratio, where (*R,M,S*)/(*S,P,R*)-**2** diastereoisomer is present in the largest amount. The NMR data shows up to four signals for most of the resonances in complex 2, including the most characteristic such as two protons of the iridanaphthalene unit, the methoxy group or C_α, C_β and C_γ (see a selection in Figure 1).

The four sets of signals stem from the three different diastereoisomers and the fact that the (*R,M,S*)/(*S,P,R*)-**2** do not present any symmetry element and therefore the two orthogonal π systems may present different signals in NMR. However, the resonances of the Cp* ligand or the H_β do not distinguish among the two spirobifluorene branches and a unique resonance is observed for the isomer (*R,M,S*)/(*S,P,R*)-**2**. In addition, the $^{31}P\{^1H\}$ NMR spectrum only displays two signals as the phosphine ligands are less affected by the stereochemistry of the system and the $^{31}P\{^1H\}$ NMR spectrum is less sensitive than the ^1H NMR spectrum.

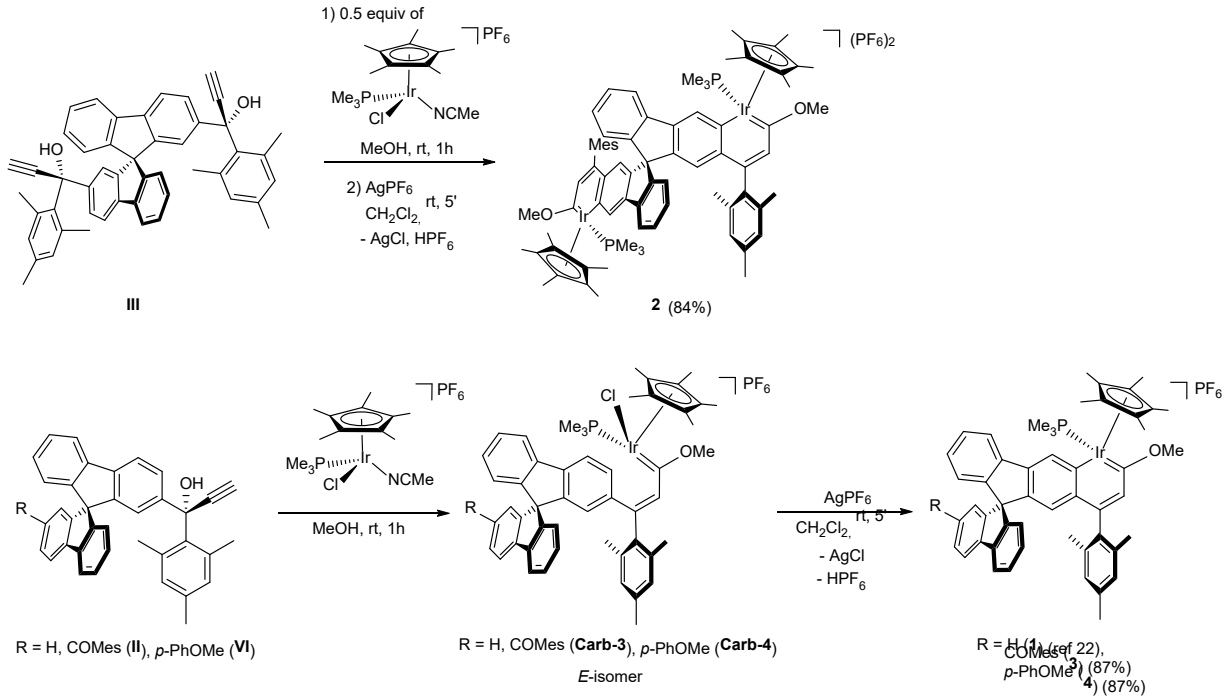

Scheme 1. Synthesis of complex **2** (top) and complexes **1**, **3** and **4** (bottom). For clarity, only one possible stereoisomer of each complex has been depicted. Mes = mesityl = 2,4,6-trifmethylbenzene

Interestingly, at 300 MHz, hindered rotation about the biaryl bond between the iridanaphthalene moiety and the mesityl substituent, is observed through the ^{1}H NMR non-equivalent *ortho*-methyl groups for only one isomer. However, when measuring at 500 MHz, all the diastereoisomers display such diastereotopic character as it was detected for compound **1**.[22]

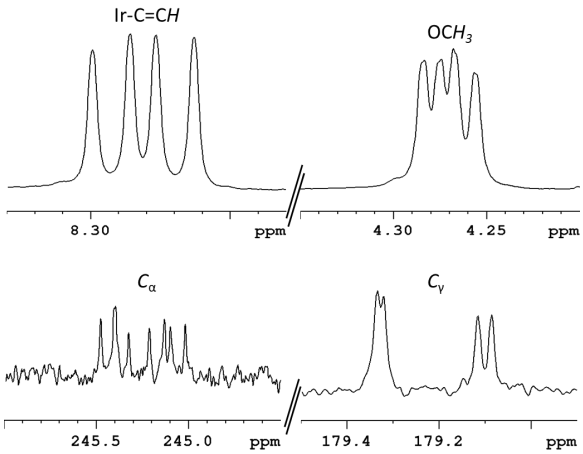

Figure 1. ^{1}H NMR (300 MHz) and ^{13}C JMOD (500 MHz, J-modulated spic echo) spectra of the diastereoisomers mixture of complex **2** in CD_2Cl_2 showing four singlets for all the resonances except the C_α which displays four doublets ($^{2}J_{CP}$ = 10.9 Hz).

However, compounds **3** and **4**, which also present the chiral axis, only bear one iridium atom in the molecule and therefore, only two pairs of enantiomers (*R,P*)/(*S,M*) and (*R,M*)/(*S,P*) are expected and observed by ^{1}H and ^{13}C{^{1}H} NMR analysis. In both cases, the presence of both diastereoisomers was equally observed with a ≈1:1 ratio. Contrary to complex **2**, the hindered rotation about the C_γ-mesityl biaryl bond is already visible at 300 MHz for both diastereoisomers.

Slow evaporation in air of compounds **2** and **3** in a CH_2Cl_2/hexane mixture gave rise to single crystals of (*R,M,S*)/(*S,P,R*)-**2** and (*R,P*)/(*S,M*)-**3**, both suitable for solid state study by X-ray diffraction analysis which confirms the proposed formulation and solution characterization (Figure 2). The structural data of the complexes are like other iridanaphthalene compounds.[22, 30, 32, 33] Thus, the metallacycle presents an almost planar structure with a deviation of the iridium atom of less than 0.5Å. In addition, the bond lengths of Ir–C bonds are between 1.964 and 2.047Å, comparable to other iridanaphthalene compounds.[22, 30, 32, 33] Finally, the aromaticity of both complexes is supported by the C–C bond lengths of the iridium aromatic ring with values between 1.354 and 1.461Å similar to those of the other benzene moieties at the complexes.

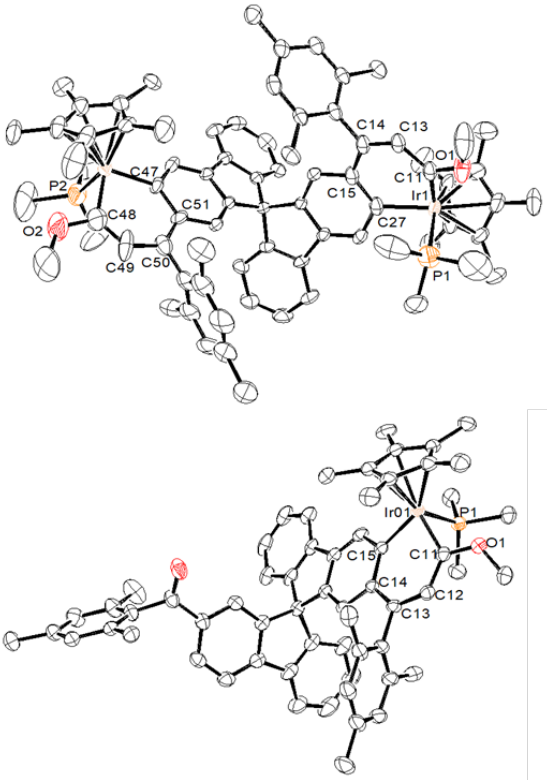

Figure 2. ORTEP representation of cation complexes (*R,M,S*)/(*S,P,R*)-**2** (top) and (*R,P*)/(*S,M*)-**3** (bottom) with thermal ellipsoids drawn at 50% probability level. All hydrogen atoms have been omitted for clarity. Selected bonds (Å) and angles (°) for complex **2**: Ir(1)-P(1) 2.282(2), Ir(2)-P(2) 2.280(2), Ir(1)-C(11) 1.984(7), C(13)-C(11) 1.448(11), C(13)-C(14) 1.366(11), C(14)-C(15) 1.461(12), C(15)-C(27) 1.416(11), Ir(1)-C(27) 2.047(6), C(48)-Ir(2) 1.952(9), C(48)-C(49) 1.354(17), C(49)-C(50) 1.366(13), C(50)-C(51) 1.438(12), C(47)-C(51) 1.443(11), C(47)-Ir(2) 2.056(6), C(11)-Ir(1)-C(27) 88.7(3), C(48)-Ir(2)-C(47) 91.5(3). Selected bonds (Å) and angles (°) for complex **3**: Ir(1)-P(1) 2.183(6), Ir(1)-C(11) 1.964(3), C(12)-C(11) 1.425(6), C(12)-C(13) 1.365(6), C(13)-C(14) 1.452(5), C(14)-C(15) 1.431(5), Ir(1)-C(15) 2.050(3), C(11)-Ir(1)-C(15) 89.71(14), C(11)-Ir(1)-P(1) 86.38(10).

The aromaticity of all diastereoisomers of **2**, **3** and **4** have been confirmed by the NMR data, the X-ray diffraction structures of two of them as experimental methodologies (see above).[1] Also, the anisotropy of the current-induced density (ACID) calculations, one of the most widely used theoretical method for aromaticity,[34] was performed. The ACID isosurface for the different isomers of **2**, **3** and **4** show a clear aromatic character with CIV values (critical isosurface values)[35] for the cycle with the iridium atom (Figure 3, Table 1) similar to the previously published spirobifluorene iridaaromatic complex **1** with a value of 0.060.[22] If the iridium atom is exchange by a CH unit, the CIV values increase as the aromaticity of iridium systems is slightly lower. In addition, nucleus-independent chemical shift (NICS) calculations were also performed on (*S,M,S*)-**2** and the corresponding organic derivative with negative values that indicate aromaticity and confirm the results obtained by ACID (see supporting information).

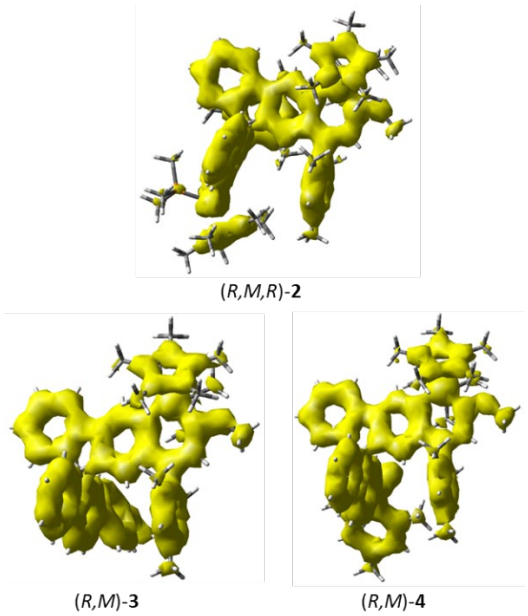

Figure 3. ACID plots of an isomer of complexes **2**, **3** and **4**.

Table 1: CIV values, first static hyperpolarizability values and theoretical electronic gap values for the isomers of compounds **2**, **3**, **4** and the corresponding organic analogue where the $[IrCp^*(PMe_3)]^+$ fragment is replaced by a CH unit.

Complex		CIV value[a]	β_{tot}×10 $^{-30}$ (esu)[b]	ΔE_{H-L} (eV)
1	1	0.060[c]	43.0	2.57
	Org	0.070[c]	3.4	4.08
2	(*R,M,R*)	0.050	35.9	2.95
	(*R,M,S*)	0.050/0.058	41.5	2.94
	(*S,M,S*)	0.054	46.9	2.93
	Org	0.063	2.0	4.02
3	(*R,M*)	0.050	40.8	2.72
	(*R,P*)	0.054	39.2	2.68
	Org	0.060	12.5	3.66
4	(*R,M*)	0.054	42.8	2.02
	(*R,P*)	0.049	45.0	2.00
	Org	0.066	10.2	4.04

[a]Values for the cycle of the iridium atom or the replacement CH unit. [b]CAM-B3LYP level of theory. [c]See ref 22.

Thermogravimetric analysis (TGA) of the stereoisomeric mixtures of iridaaromatic complexes **2**, **3** and **4** show high thermal stability as the initial decomposition temperature measured at the 5% mass loss point are 533 K, 583 K and 523 K respectively. These stabilities are considerably higher than that of complex **1**, 473 K.[22] Particularly, the increase in thermal stability of 60 K for complex **2** compared to **1** may be attributed to the larger aromatic system present in **2**.

The UV-vis absorption spectra (Figure 4), in dichloromethane with a concentration of $6{\cdot}10^{-5}$ M, of the stereoisomeric mixtures of **2**, **3** and **4** show two bands where the maximum wavelength for the first band is 271 nm (ε=19000 $M^{-1}cm^{-1}$), 300 nm (ε=33333 $M^{-1}cm^{-1}$) and 299 nm (ε=35069 $M^{-1}cm^{-1}$) respectively, while in the second band the maximum wavelength is 424 nm (ε=17500 $M^{-1}cm^{-1}$), 426 nm (ε=21667 $M^{-1}cm^{-1}$) and 423 nm (ε=19416 $M^{-1}cm^{-1}$). It has been shown that the introduction of an iridanaphthalene in one of the SBF branches provokes a red-shift of the maximum wavelength with respect to its organic analogue.[22] However, a second iridium atom, meaning an iridanaphthalene in each fluorene branch, as shown in complex **2**, has no clear effect with respect to complex **1**. Although compounds **3** and **4** whose second fluorene branch is substituted with a ketone or a methoxyphenyl group have similar wavelengths to the other iridaaromatic systems, they clearly show a large effect on absorptivity.

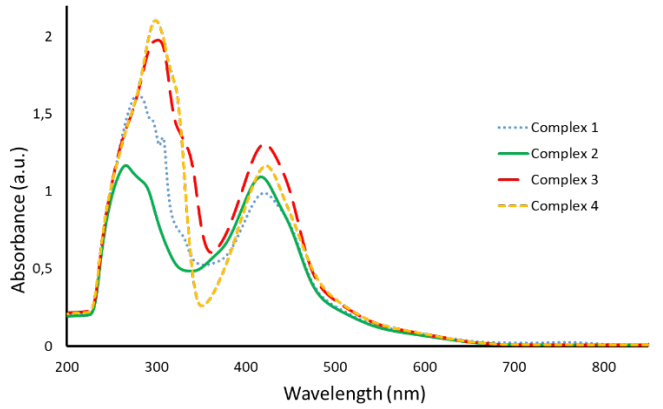

Figure 4. UV-Vis spectra of complexes **1-4** in CH_2Cl_2 ($6{\cdot}10^{-5}$ M).

To better understand the experimental UV-Vis spectra, time-dependent density functional theory (TD-DFT) calculations were performed for **1**, and for each of the diastereoisomers of **2**, **3** and **4** at the CAM-B3LYP level. The theoretical UV-vis spectra show no differences between the respective diastereoisomer for each of the compounds. Thus, the bands at 424 nm of complex **2** is assigned to the electronic transitions HOMO→LUMO while in compound **3** band at 300 is assigned to the transition HOMO→LUMO+1 and the band at 426 nm to HOMO→LUMO and HOMO-3→LUMO. Finally, for complex **4** assignments are to HOMO→LUMO+3 and HOMO-1→LUMO for bands at 299 and 423 nm respectively. Notably, the theoretical spectra show a redshift of 143 nm for complex **2**, 120 nm for **3** and 146 nm for **4** with respect to their organic analogues where the iridium fragment is replaced by a CH unit.

The experimental UV-Vis absorption measurements allowed to determine the optical bandgaps through Tauc's plot from the lowest electronic absorption. Thus, the direct band gap for complex **1** and the mixtures of diastereoisomers of **2**, **3**, and **4** are 2.37, 2.51, 2.39 and 2.30 eV, respectively. These optical band gaps value allow to determine that the complexes **1**-**4** are transparent in a 1.8-2.4 eV range of the UV-Vis approximately.

Theoretical studies can be used to predict the NLO behaviour on molecular systems. Different studies indicate that the first hyperpolarizability values calculated by the DFT CAM-B3LYP functional are more accurate than those obtained by B3LYP functional.[18, 36] Thus, the first hyperpolarizability (β_{tot}x10^{-30} esu) of compounds **1**, **2**, **3** and **4** was determined using CAM-B3LYP functional (See table 1). The data obtained revealed that the introduction of the iridium fragment in comparison with the

organic analogue effectively improves the first hyperpolarizability, its values being much higher, probably due to the modification on the electronic distribution. Thus, the β_{tot} values of complex **2** diastereoisomers are 35.9, 41.5 and 46.9 while the exchange of the iridium atom by a CH unit drastically reduces the first hyperpolarizability to 2. Although theoretical studies suggest that the introduction of iridium may effectively improve the second-order NLO responses, it should also be noted that the introduction of two iridium fragments versus the introduction of one iridium fragment does not show a marked difference in the NLO response, as the exchange of only one of the iridium atoms by a CH unit led to a β_{tot} of 41. In addition to introducing an iridium fragment to boost the first order hyperpolarizability, and therefore, the NLO properties, another strategy would be the incorporation of donor or acceptor groups to increase the electron-donor or acceptor ability of the system.[18, 37, 38] Thus, complex **3** and **4** allowed to study the effect of acceptor or donor groups, respectively, in the second fluorene branch. However, the introduction of these groups practically does not affect the β_{tot} predicted values, which seems to be in accordance with the lack of spiroconjugation in these complexes. Even so, it can be said that the complexes studied here have good second-order NLO responses.

Other electronic properties as low HOMO-LUMO energy gaps and intramolecular charge transfer (ICT) have been directly related to NLO properties. In order to study the molecular electronic mobility, the frontier molecular orbitals (FMOs) analysis has been shown as an important tool.[18] Thus, for complex **3**, the HOMO is localized on the ketone substituent on the SBF branch while the LUMO is extended over the SBF branch with the iridium atom. Similarly, the MOs of complex **4** show the HOMO at the fluorene branch with the methoxyphenyl substituent and the LUMO at the iridaaromatic branch. In contrast, in complex **2** the FMOs distribution is in the two orthogonal pi systems. Additionally, while HOMO presents homogeneous distribution over the whole π-systems, LUMO is more concentrated on the aromatic ring containing the iridium metal atom, this can be considered as intramolecular charge transfer (Figure 5 and SI).

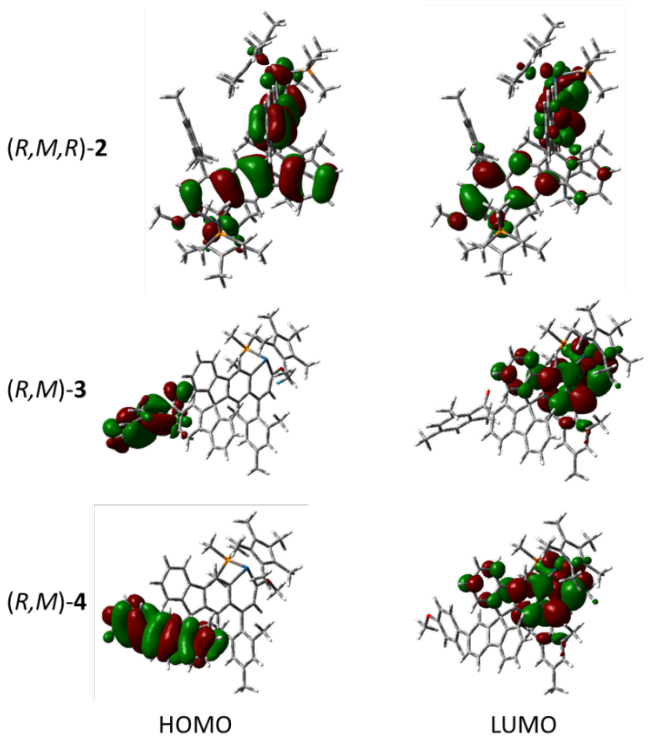

Figure 5. HOMO and LUMO representation of some diastereoisomers of complexes **2**, **3** and **4**. Isovalue 0.02.

The HOMO-LUMO energy gaps obtained for compounds **1**, **2**, **3** and **4** are lower than their organic analogues which shows a clear influence of the iridium fragment (Table 1). While for complex **2** and **3** the gap difference respect to their organic analogue is around 1-1.1 eV, for complex **1** it increases to 1.5 eV and for complex **4** there is a gap difference of 2 eV. This shows that the introduction of an iridium fragment in one fluorene branch and a donor group in the other fluorene branch has a greater influence on the HOMO-LUMO energy gap values. In addition, the low value display by complex **3** suggests a clear semiconductor behaviour.

Finally, the electrochemical properties of compounds **1**-**4** were studied by cyclic voltammetry (CV) in dichloromethane (see SI for full details). The features of voltammograms for these compounds are similar, exhibiting two electrochemical events. On the cathodic side, one reversible reduction is observed for complexes **1**, **3** and **4**. In contrast, complex **2** exhibits two separate, but very close, reversible reduction waves which could be assigned to the two iridium atoms (Figure 6). This electrochemical process was attributed to the Ir(III)/Ir(II) reduction as previously observed for other Ir(III) complexes.[39, 40] This assignment is supported by DFT calculations since the LUMO of complexes **3** and **4** is localized over the SBF branch with the iridium atom (see above). On the anodic side, one quasi-reversible oxidation is observed for all complexes (Figure 6) probably related to the organic fragment since the propargylic alcohols used for the synthesis of complexes **1**-**4** undergo an oxidation in the anodic potential range. This fact is also suggested by DFT calculations since the HOMO, from which

the electron is lost, is located at the fluorene branch with ketone (**3**) or methoxyphenyl group (**4**).

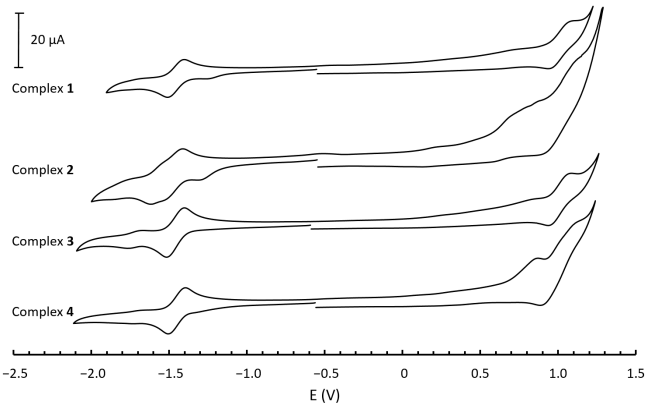

Figure 6. Cyclic voltammograms of 1mM solutions of complexes **1-4** in CH_2Cl_2, with 0.1 M tetrabutylammoniumhexafluorophosphate ($TBAPF_6$) as supporting electrolyte. Scan rate: 0.2 V/s

On the cathodic scan, a reversible reduction with $E_{1/2}$ around −1.45 V vs. Fc/Fc^+ was observed for all the complexes, and a second one with $E_{1/2}$ around −1.59 V vs. Fc/Fc^+ (Table 2). In addition, on the anodic scan, an oxidation with $E_{1/2}$ around 1 V vs. Fc/Fc^+ was also observed for all the complexes. Therefore, the similar redox behavior in compounds **1**, **3** and **4** indicates that the substituents on the second fluorene unit do not exert a significant effect on the electronic states. Likewise, although the introduction of the second iridium fragment leads to the appearance of a second nearly overlapped reduction wave, it does not modify any other characteristics.

Table 2. Optical gaps and relevant electrochemical data.

Complex	$E_{1/2}$ (V)	ΔE_p (V)[a]	$E_{CV\ gap}$ (eV)[b]	$E_{optical\ gap}$ (eV)
1	-1.45	0.10	2.34	2.37
	1.02	0.15		
2	-1.46	0.11	2.33	2.51
	-1.59	0.05		
	1.01	0.20		
3	-1.45	0.11	2.36	2.39
	-1.74	0.09		
	1.00	0.15		
4	-1.45	0.12	2.29	2.30
	-1.74	0.10		
	1.00	0.25		

[a] $\Delta E_p = E_{pa}-E_{pc}$; [b] $E_{CV\ gap} = E_{HOMO}-E_{LUMO}$: E_{LUMO} (eV) = − ($E_{onset,\ red}$ + 5.1); E_{HOMO} (eV) = − ($E_{onset,\ oxid}$ + 5.1). Both are determined vs. $E_{Fc+/Fc}$[41-43]

The effect of the scan rate on the electrochemical response was investigated between 0.1 and 1 V/s. For all complexes first reduction processes, the peak-to-peak separation (ΔE_p) values was about 110 mV at 0.2 V/s (Table 2), and ΔE_p values from 0.09 to 170 mV were observed in relation to changes in the scan rate. Furthermore, the ratio of cathodic to anodic peak currents (i_{pc}/i_{pa}) remained close to unit. These parameters are in accordance to the Fc/Fc^+ redox couple under the same experimental conditions which suggests a reversible charge transfer process.[41] In addition, for all redox processes a linear dependence of peak current on the square root of the scan rate was observed, which is indicative of the diffusion-controlled nature of the processes (see SI). Altogether, the iridium reduced state of complexes **1-4** is stable on the timescale of electrochemical experiments.

Finally, the HOMO–LUMO gaps were obtained from the CV experiments with values around 2.3 eV for all the compounds. These values are nearly identical to the optical band gaps (Table 2) and similar to the theoretical values (Table 1). Thus, the complexes **1**-**4** can classify among the semiconductors for applications in photovoltaics and optoelectronics.

Conclusions

In conclusion, the synthesis and characterization of three new spirobifluorene iridanaphthalene complexes, including the first complex with two iridaaromatic systems into the π skeleton of a SBF moiety has been achieved. In addition, their electronic and optical properties have been studied through both experimental and theoretical approaches demonstrating a great influence of the systems by introducing an iridium atom in the aromatic moiety. They have shown that complexes **1**-**4** present not only transparency in the 1.8-2.4 eV UV-Vis range, but also a semiconductor behaviour. Additionally, non-linear optical properties are predicted with first hyperpolarizability values considerably higher than the organic analogues. Notably, these complexes show high stability under air, at high temperatures and in electrochemical conditions. This work demonstrates that metallaaromatic complexes within the π skeleton of a spirobifluorene are suitable building blocks for new organometallic structures where electrical and optical properties can be modulated for semiconductors, optical or electrooptical devices.

Author Contributions

Conceptualization, M.T. and S. B.; investigation, M.T., R.P-C., A. P-G., I.V-C. and I.P.; formal analysis, A.P-G.; writing—original draft preparation, M.T. and S.B.; writing—review and editing, all.; supervision and funding acquisition, S.B.

Conflicts of interest

There are no conflicts to declare.

Acknowledgements

A.P-G. thanks Xunta de Galicia for the GRC2019/24 project and Dr Herges for the ACID program. S. B., J. A-G, R.P-C. and M. T. thank the FA3 group of the University of Vigo for all the support. All authors are thankful to the University of Vigo CACTI services for recording the NMR and MS spectra and the X-ray data.

Notes and references

1. D. Chen, Y. Hua and H. Xia, *Chem. Rev.*, 2020, **120**, 12994-13086.
2. B. J. Frogley and L. J. Wright, *Chem. Eur. J.*, 2018, **24**, 2025-2038.
3. B. J. Frogley and L. J. Wright, *Coord. Chem. Rev.*, 2014, **270-271**, 151-166.
4. G. Jia, *Organometallics*, 2013, **32**, 6852-6866.
5. M. Talavera and S. Bolaño, *Molecules*, 2021, **26**, 4655.
6. Y. Zhang, C. Yu, Z. Huang, W.-X. Zhang, S. Ye, J. Wei and Z. Xi, *Acc. Chem. Res.*, 2021, **54**, 2323-2333.
7. C. Zhu, S. Li, M. Luo, X. Zhou, Y. Niu, M. Lin, J. Zhu, Z. Cao, X. Lu, T. Wen, Z. Xie, P. v. R. Schleyer and H. Xia, *Nat. Chem.*, 2013, **5**, 698-703.
8. R. Li, Z. Lu, Y. Cai, F. Jiang, C. Tang, Z. Chen, J. Zheng, J. Pi, R. Zhang, J. Liu, Z.-B. Chen, Y. Yang, J. Shi, W. Hong and H. Xia, *J. Am. Chem. Soc.*, 2017, **139**, 14344-14347.
9. Z. Lu, Q. Lin, Y. Cai, S. Chen, J. Chen, W. Wu, X. He and H. Xia, *ACS Macro Lett.*, 2018, **7**, 1034-1038.
10. H. Zhang, H. Zhao, K. Zhuo, Y. Hua, J. Chen, X. He, W. Weng and H. Xia, *Polym. Chem.*, 2019, **10**, 386-394.
11. Y. Chen, L. Yang, W. Zheng, P. Ouyang, H. Zhang, Y. Ruan, W. Weng, X. He and H. Xia, *ACS Macro Lett.*, 2020, **9**, 344-349.
12. J. Wang, J. Li, Y. Zhou, C. Yu, Y. Hua, Y. Yu, R. Li, X. Lin, R. Chen, H. Wu, H. Xia and H.-L. Wang, *J. Am. Chem. Soc.*, 2021, **143**, 7759-7768.
13. L. Liu, S. Chen, Y. Qu, X. Gao, L. Han, Z. Lin, L. Yang, W. Wang, N. Zheng, Y. Liang, Y. Tan, H. Xia and F. He, *Adv. Mater.*, 2021, **33**, 2101279.
14. S. Castro-Fernández, R. Yang, A. P. García, I. L. Garzón, H. Xu, A. G. Petrovic and J. L. Alonso-Gómez, *Chem. Eur. J.*, 2017, **23**, 11747-11751.
15. A. Ozcelik, R. Pereira-Cameselle, A. von Weber, M. Paszkiewicz, M. Carlotti, T. Paintner, L. Zhang, T. Lin, Y. Q. Zhang, J. V. Barth, T. van den Nobelen, R. C. Chiechi, M. Jakob, U. Heiz, S. Chiussi, A. Kartouzian, F. Klappenberger and J. L. Alonso-Gómez, *Langmuir*, 2018, **34**, 4548-4553.
16. Y. Si, G. Yang and Z. Su, *J. Mater. Chem. C*, 2013, **1**, 1399-1406.
17. T. Michinobu, J. C. May, J. H. Lim, C. Boudon, J.-P. Gisselbrecht, P. Seiler, M. Gross, I. Biaggio and F. Diederich, *Chem. Commun.*, 2005, **2005**, 737-739.
18. Y. Si and G. Yang, *J. Phys. Chem. A*, 2014, **118**, 1094-1102.
19. A. Ozcelik, R. Pereira-Cameselle, Á. Peña-Gallego and J. L. Alonso-Gómez, *Eur. J. Org. Chem.*, 2022, **2022**, e202101333.
20. L. R. Dalton, P. A. Sullivan and D. H. Bale, *Chem. Rev.*, 2010, **110**, 25-55.
21. C. Wang, T. Zhang and W. Lin, *Chem. Rev.*, 2012, **112**, 1084-1104.
22. V. C. Arias-Coronado, R. Pereira-Cameselle, A. Ozcelik, M. Talavera, Á. Peña-Gallego, J. L. Alonso-Gómez and S. Bolaño, *Chem. Eur. J.*, 2019, **25**, 13496-13499.
23. J. Heck, S. Dabek, T. Meyer-Friedrichsen and H. Wong, *Coord. Chem. Rev.*, 1999, **190-192**, 1217-1254.
24. N. K. Nkungli and J. N. Ghogomu, *J. Theor. Chem.*, 2016, **2016**, 7909576.
25. Z. Wang, Y.-H. Fang, H. Lin, G. Zhao, W. Yan, Z. Ma, Q.-H. Li and J. Zhang, *Chin. J. Chem .* 2022, **40**, 2611-2617.
26. Z. Wang, W. Yan, G. Zhao, K. Wu, Z.-G. Gu, Q.-h. Li and J. Zhang, *J. Phys. Chem. Lett.*, 2021, **12**, 11784-11789.
27. L. Wang, J. Ye, H. Wang, H. Xie and Y. Qiu, *Sci. Rep.*, 2017, **7**, 10182.
28. A. Karton, M. A. Iron, M. E. van der Boom and J. M. L. Martin, *J. Phys. Chem. A*, 2005, **109**, 5454-5462.
29. M. Talavera, A. Peña-Gallego, J. L. Alonso-Gómez and S. Bolaño, *Chem. Commun.*, 2018, **54**, 10974-10976.
30. M. Talavera, J. Bravo, J. Castro, S. Garcia-Fontan, J. M. Hermida-Ramon and S. Bolano, *Dalton Trans*, 2014, **43**, 17366-17374.
31. M. Talavera, K. M. Cid-Seara, A. Peña-Gallego and S. Bolano, *Dalton Trans.*, 2021, **50**, 11216-11220.
32. M. Talavera, S. Bolaño, J. Bravo, J. Castro, S. García-Fontán and J. M. Hermida-Ramón, *Organometallics*, 2013, **32**, 4058-4060.
33. Á. Vivancos, Y. A. Hernández, M. Paneque, M. L. Poveda, V. Salazar and E. Álvarez, *Organometallics*, 2015, **34**, 177-188.
34. D. Geuenich, K. Hess, F. Köhler and R. Herges, *Chem. Rev.*, 2005, **105**, 3758-3772.
35. , CIV value refers to the isosurface value at which the ACID surface breaks. The higher the CIV, the stronger is the conjugation.
36. S. J. A. v. Gisbergen, J. G. Snijders and E. J. Baerends, *J. Chem. Phys.*, 1998, **109**, 10657-10668.
37. S. Y. Kim, M. Lee and B. H. Boo, *J. Chem. Phys.*, 1998, **109**, 2593-2595.
38. D. R. Kanis, M. A. Ratner and T. J. Marks, *Chem. Rev.*, 1994, **94**, 195-242.
39. R. Acharyya, F. Basuli, R.-Z. Wang, T. C. W. Mak and S. Bhattacharya, *Inorg. Chem.*, 2004, **43**, 704-711.
40. Y. Qin, Q. Zhu, R. Sun, J. M. Ganley, R. R. Knowles and D. G. Nocera, *J. Am. Chem. Soc.*, 2021, **143**, 10232-10242.
41. A. J. Bard and L. R. Faulkner, *Electrochemical Methods: Fundamentals and Applications*, 2nd edn., 2001.
42. W. N. Hansen and G. J. Hansen, *Phys. Rev. A*, 1987, **36**, 1396-1402.
43. S. Trasatti, *Pure Appl. Chem.*, 1986, **58**, 955-966.